RESEARCH ARTICLE

ADVANCED MATERIALS INTERFACES
www.advmatinterfaces.de

Electronic Doping and Enhancement of n-Channel Polycrystalline OFET Performance through Gate Oxide Modifications with Aminosilanes

*Nara Shin, Karl Sebastian Schellhammer, Min Ho Lee, Jakob Zessin, Mike Hambsch, Alberto Salleo, Frank Ortmann, and Stefan C. B. Mannsfeld**

Self-assembled monolayers (SAMs) are widely employed in organic field-effect transistors to modify the surface energy, surface roughness, film growth kinetics, and electrical surface potential of the gate oxide to control the device's operating voltage. In this study, amino-functionalized SAM molecules are compared to pure alkylsilane SAMS in terms of their impact on the electrical properties of organic field-effect transistors, using the n-type polycrystalline small molecule semiconductor material *N*,*N′*-dioctyl-3,4,9,10-perylenedicarboximide (PTCDI-C8). In order to understand the electronic impact of the amino groups, the effect of both the number of amino-containing functional groups and the SAM molecular length are systematically studied. Though amino-functionalized SAM materials have been studied previously, this study is, for the first time, able to shed light on the nature of the doping effect that occurs when the gate oxide is treated with polar aminosilane materials. By a comprehensive theoretical study of the interface on the molecular level, it is shown that the observed shift in the threshold voltage is caused by free charges, which are attracted to the PTCDI-C8 and are stabilized there by protonated aminosilanes. This attraction and the voltage shift can be systematically tuned by varying the length of the neutral terminal chain of the aminosilane.

1. Introduction

Chemical modification of gate dielectric surfaces is one of the simple and efficient ways to attempt to control electrical performance of organic field-effect transistors (OFETs). The chemical and physical properties of the interface between gate dielectric layer and organic semiconductors (OSCs) directly affect the OSC-layer growth and thus the charge carrier mobility.[1,2]

For optimized performance, the gate oxide surface is functionalized with self-assembled monolayers (SAMs). SAMs have been applied for OFETs to facilitate micro-patterning,[3,4] to enable chemical sensing,[5] to modify the gate oxide surfaces' physical properties,[6] and to induce additional charges.[7–9] Using different types of SAMs on the same gate dielectric has even enabled the fabrication of pseudo-complementary circuits with one (ambipolar) semiconducting material by controlling the injection efficiency of different carrier types into the film with the different functional groups.[10,11]

Previous studies reported that the surface energy and roughness of the gate dielectric mainly influence the grain growth of OSCs including the molecular orientation/ordering and the grain size/connectivity.[1,12–15] A gate oxide modification with SAM materials inevitably involves the change of the OSC morphology affecting the carrier mobility of the device.[1,16,17] Since the conducting channel is formed near the gate dielectric, the molecular orientation and ordering of the first OSC layer have a significant impact on the electrical transport properties[18–20] as well as the growth kinetics of the next layer, offering potential

Dr. N. Shin, Dr. K. S. Schellhammer, J. Zessin, Dr. M. Hambsch, Prof. F. Ortmann, Prof. S. C. B. Mannsfeld
Center for Advancing Electronics (cfaed)
Technische Universität Dresden
01062 Dresden, Germany
E-mail: stefan.mannsfeld@tu-dresden.de

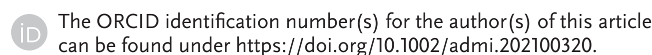
The ORCID identification number(s) for the author(s) of this article can be found under https://doi.org/10.1002/admi.202100320.

© 2021 The Authors. Advanced Materials Interfaces published by Wiley-VCH GmbH. This is an open access article under the terms of the Creative Commons Attribution-NonCommercial-NoDerivs License, which permits use and distribution in any medium, provided the original work is properly cited, the use is non-commercial and no modifications or adaptations are made.

DOI: 10.1002/admi.202100320

Dr. N. Shin, Dr. M. Hambsch, Prof. S. C. B. Mannsfeld
Faculty of Electrical and Computer Engineering
Technische Universität Dresden
01062 Dresden, Germany

Dr. M. H. Lee
Leibniz-Institute for Solid State and Materials Research Dresden (IFW Dresden)
Helmholtzstr. 20, 01069 Dresden, Germany

Prof. A. Salleo
Department of Materials Science and Engineering
Stanford University
496 Lomita Mall, Stanford, CA 94305, USA

Prof. F. Ortmann
Department of Chemistry
Technische Universität München
Lichtenbergstr. 4, 85748 Garching b. München, Germany

 © 2021 The Authors. Advanced Materials Interfaces published by Wiley-VCH GmbH

pathways for charge carriers by vertical bridging across the grain boundaries in the first layer.[21]

Therefore, modifications of the gate oxide surface with SAMs have been the most common approach to effectively control the surface properties, as the SAM molecules largely dictate the surface energy and roughness seen by a subsequently deposited OSC material.[22–24] Among various SAM materials, alkylsilanes and in particular the octadecylsilane materials (octadecyltrimethoxysilane and octadecyltrichlorosilane, so-called "ODTS") are probably the most commonly used SAMs to modify the surface properties of the gate oxide.[13,25] Since the ODTS-treated gate oxide layer has a low surface energy due to the hydrophobic nature of the ODTS' terminal CH_3 groups, the crystal quality of OSCs on ODTS-treated silicon oxides has been found to be increased, and continuous 2D growth mode of OSCs has been observed rather than discontinuous 3D growth mode.[22,26] The density of water trap states in the channel—a common cause of mobility reduction[27] and operating voltage increase[28]—is also reduced due to the increased surface hydrophobicity.[29] Accordingly, transistors fabricated on ODTS-treated gate oxide usually show higher carrier mobility than on bare gate oxide. For example, pentacene FETs fabricated on ODTS-treated gate oxides resulted in a field-effect mobility of 1.5 $cm^2 V^{-1} s^{-1}$, while bare gate oxide devices showed field-effect mobilities of 0.7 $cm^2 V^{-1} s^{-1}$.[30,31] Using ODTS-treated SiO_2/Si also enhanced the electron mobility of *N,N´*-bis(cyclohexyl)naphthalenediimide FETs from 0.0001 to 6.2 $cm^2 V^{-1} s^{-1}$.[32] However, most of such studies that investigated the effects of SAM-treated surfaces on the OSC growth and the electrical performances have focused on p-type OSCs such as pentacene,[12,33] poly(3-hexylthiophene) (P3HT),[34] poly[bis(4-phenyl)(2,5,6-trimethylphenyl) amine (PTAA),[35] diketopyrrolopyrrole-based polymers,[20] and dihexylsexithiophene based molecules (DH6T).[36]

In this study, we investigate the performances of OFETs based on the n-type polycrystalline OSC *N,N´*-dioctyl-3,4,9,10-perylenedicarboximide (PTCDI-C8) in devices with SAM-functionalized gate dielectrics for a series of aminosilanes (A-SAMs) with different numbers of amine groups and compare these findings to devices that use conventional alkylsilanes (C-SAMs). For that purpose, A-SAMs and C-SAMs were grown on Si wafers with 300 nm SiO_2 to determine the effects of the length of alkyl chain and the number of amino groups in SAMs on the morphology and the electrical performances of PTCDI-C8 FETs.

Another important aspect of this work is to determine the role of the amino group in the observed doping effect as evidenced by threshold voltage shifts in OFET devices. Gate oxide modifications with polar SAM materials have shown to be effective in controlling threshold voltages.[37,38] Gate oxides treated with SAM molecules comprising different terminal functional groups such as fluorine and amino groups were previously found to strongly modulate the threshold voltage.[11,35,37,39] However, most of these studies only compared the threshold voltage shifts in OFETs when using F-SAM, C-SAM, and A-SAM-treated surfaces relative to one another,[35,37] but did not systematically study the role and impact of the chemical amino group in the A-SAM material itself.

Celle et al. studied the effect of interface dipoles on the threshold voltage and carrier mobility of various OFETs for many different SAM materials including mercaptosilanes (S-SAMs) and aminosilanes (A-SAMs).[2] They suggest that the dipole moments of each SAM affect the threshold voltage while they do not influence the carrier mobility in both OFETs fabricated on S-SAM or A-SAM-treated substrates. On the other hand, SAMs which consist of CH_3 functional groups (C-SAMs) possess a theoretically calculated dipole moment close to zero.[35,37] Kobayashi et al. reported that the threshold voltage values of pentacene and C_{60} FETs were shifted positively when holes are accumulated by fluoroalkyl SAMs (F-SAMs), and were shifted negatively when electrons are accumulated by A-SAMs, while this carrier accumulation effect was not significant in C-SAMs.[37] The calculated molecular dipole values could explain the threshold voltage shift of OFETs fabricated on F-SAMs and C-SAM-treated gate oxides but could not explain the increased electron accumulation in OFETs fabricated on A-SAM-treated substrates. Thus, Kobayashi et al. proposed direct weak charge transfer between organic layers for the case of A-SAMs. Gholamrezaie et al. also studied the threshold voltage shift by using F-SAMs, C-SAMs, and A-SAMs deposited on the gate oxide surfaces.[35] They claimed that the threshold voltages of PTAA FETs were shifted due to charge trapping effects that stem from the presence of the SAMs. Since the surface potential values of the SAM-treated surfaces measured by scanning Kelvin probe measurement were too high to be a result of dipole moments of SAMs they argued that the maximum surface potential values of the SAM-treated surfaces corresponded to the threshold voltage values of OFETs fabricated on each SAM-treated surface. Pernstich et al. suggested that variations in the OFET threshold voltage can be related to changes in the dielectric surface potential as induced by the dipole moment of the SAM molecules used in a gate dielectric modification.[28]

While in the above-listed works, many possible origins behind threshold voltage shifts were discussed, ranging from i) weak charge transfer effect from A-SAM to OSC materials.,[37] ii) dipole-induced addition of accumulation charges,[2,40] and iii) charge trapping effects,[35] the discussion has remained largely speculative and a deeper theoretical underpinning of these suggestions is missing so far.

In this work, this issue is addressed at least for A-SAMs by studying the electronic effects of several A-SAM materials that contain the same methoxysilane anchor group but different amino group-containing terminal groups on the OFET characteristics. To understand the origin of the observed threshold voltage shifts and their relation to the number of amino groups of the A-SAMs as well as the overall chain length, the resulting threshold voltage shifts are compared and evaluated on the basis of theoretical calculations on the molecular level electrostatic properties. Based on these calculations, we find that the dipole moment of A-SAMs that is frequently speculated to cause such threshold voltage shifts cannot satisfyingly explain the experimental results. Instead, with the combination of OFET characterization, X-ray photoelectron spectroscopy, and theoretical calculations, we are able to provide strong evidence that charge transfer between the protonated amino group of A-SAMs and the PTCDI-C8 molecule causes the observed threshold voltage shifts.

2. Result and Discussion

2.1. Surface Treatment and Characterization

Figure 1a,b show the chemical structure of employed SAM materials schematically. We used a variety of SAMs from

© 2021 The Authors. Advanced Materials Interfaces published by Wiley-VCH GmbH

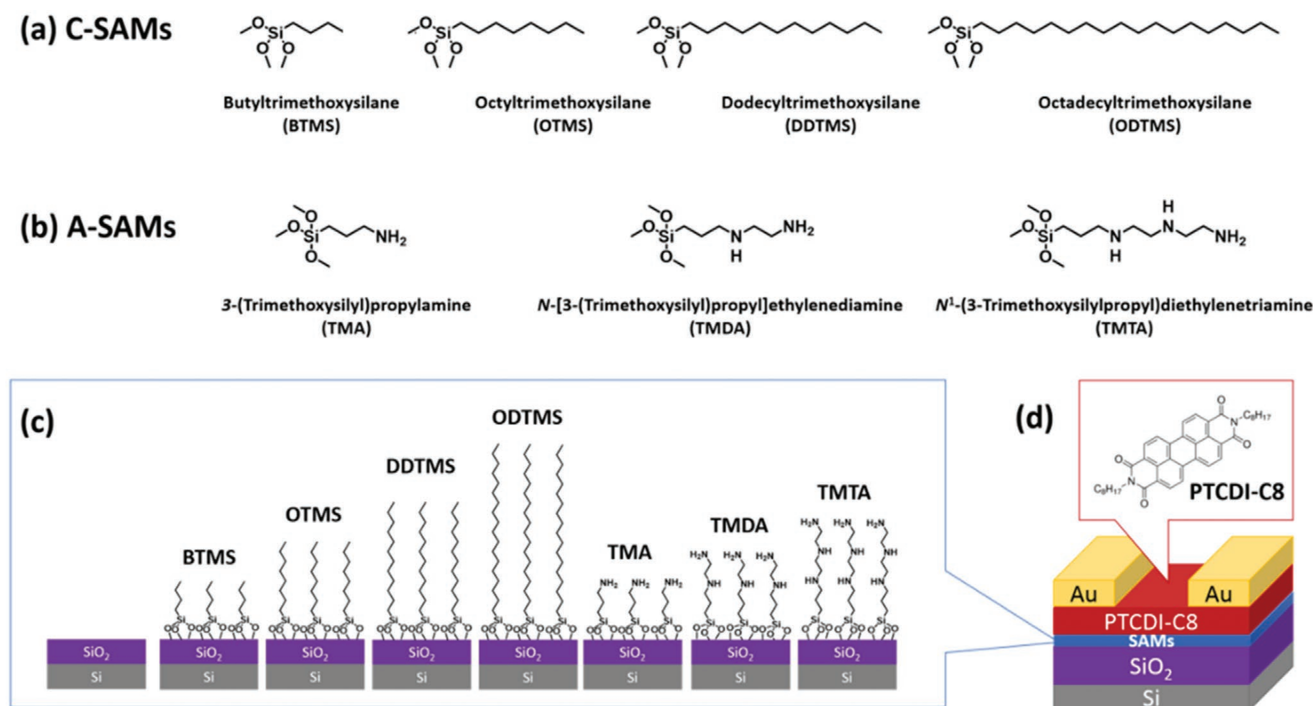

Figure 1. a) Chemical structure of C-SAMs (BTMS, OTMS, DDTMS, and ODTMS) and b) A-SAMs (TMA, TMDA, and TMTA). c) Schematic illustration of various SAM-treated SiO_2/Si substrates. d) Chemical structure of PTCDI-C8 and schematic of the bottom-gate top-contact PTCDI-C8 OFET geometry with SAM-treated substrate.

C-SAMs to A-SAMs such as BTMS, OTMS, DDTMS, ODTMS, TMA (one amino group), TMDA (two amino groups), and TMTA (three amino groups) to systematically compare the effect of the length of alkyl chain and the number of amino groups on SAMs on the morphology and the electrical performances of OFETs. The SAMs were grown on heavily doped Si wafers with a 300 nm silicon dioxide (SiO_2) layer (Figure 1c). All the OFETs were fabricated in a bottom-gate top-contact geometry with the small molecule PTCDI-C8 as shown in Figure 1d. Since the dielectric surface properties have an impact on the morphology of OSC films[18,22] as well as the resulting device performance,[1,14] we characterized the surface properties of each SAM-treated oxide layer by contact angle measurement, atomic force microscopy (AFM), and Kelvin probe force microscopy (KPFM).

The water contact angle of each SAM-treated surface was found to depend on the length of alkyl chain and the number of amino groups in the SAMs as shown in **Figure 2**a,b. The contact angle increases (more hydrophobic) with increasing lengths of the alkyl chain for C-SAM-treated surfaces (40.4° for BTMS < 49.2° for OTMS < 58.7° for DDTMS < 104.4° for ODTMS). In contrast, for A-SAM-treated surfaces, the contact angle decreases (more hydrophilic) with increasing numbers of amino group on the A-SAM molecule despite the increase in the length of alkyl chain (56.7° for TMA > 54.2° for TMDA > 49.4° for TMTA). This is possibly due to the fact that the terminal CH_3 group of C-SAMs is non-polar and thus hydrophobic while the terminal NH_2 group of A-SAMs is polar (due to the electronegativity of the N atom) and can form hydrogen bonds with water molecules.

Figure 2c–j show the AFM topography recorded for each SAM-treated oxide surface, which yields fairly smooth films with rms roughness values below 1 nm (Table S1, Supporting Information). All of the C-SAM-treated surfaces exhibit rms roughness values in a range of 0.11–0.14 nm and are thus smoother than the bare SiO_2/Si substrate with the rms roughness of 0.16 nm (0.14 nm for BTMS, 0.12 nm for OTMS, 0.11 nm for DDTMS, and 0.14 nm for ODTMS). However, the surface roughness of A-SAM-treated surfaces slightly increases with the length of alkyl chain and the number of amino groups (0.09 nm for TMA < 0.18 nm for TMDA < 0.42 nm for TMTA). Therefore, different OSC morphologies and electrical properties of OFETs fabricated on C-SAM and A-SAM-treated surfaces would be expected due to these different surface properties.[12,14]

The surface potential of each SAM-treated surface was obtained by KPFM using an additional evaporated gold reference (50 nm thickness) as depicted in Figure S1a, Supporting Information. Figure S1b, Supporting Information shows the CPD values of each SAM surface relative to that of gold as a function of the number of amino group on SAMs as calculated by integration of the signal area in each KPFM image (Figure S1c, Supporting Information). The OTMS and ODTMS-treated substrates (0.24 and 0.95 V each relative to a gold electrode) show more negative and positive values than the bare substrates (0.72 V relative to a gold electrode), respectively. It is somewhat peculiar that the difference between each surface potential value of OTMS and ODTMS-treated oxides is as large as observed here. We suspect that the surface potential value of OTMS-treated substrate and bare substrate could not be obtained precisely in air circumstances in which we measured because water molecules exist on top of the surfaces which are hydrophilic in contrast to the hydrophobic ODTMS-treated substrate. For A-SAM-treated substrates, the surface potential values are found to increase

© 2021 The Authors. Advanced Materials Interfaces published by Wiley-VCH GmbH

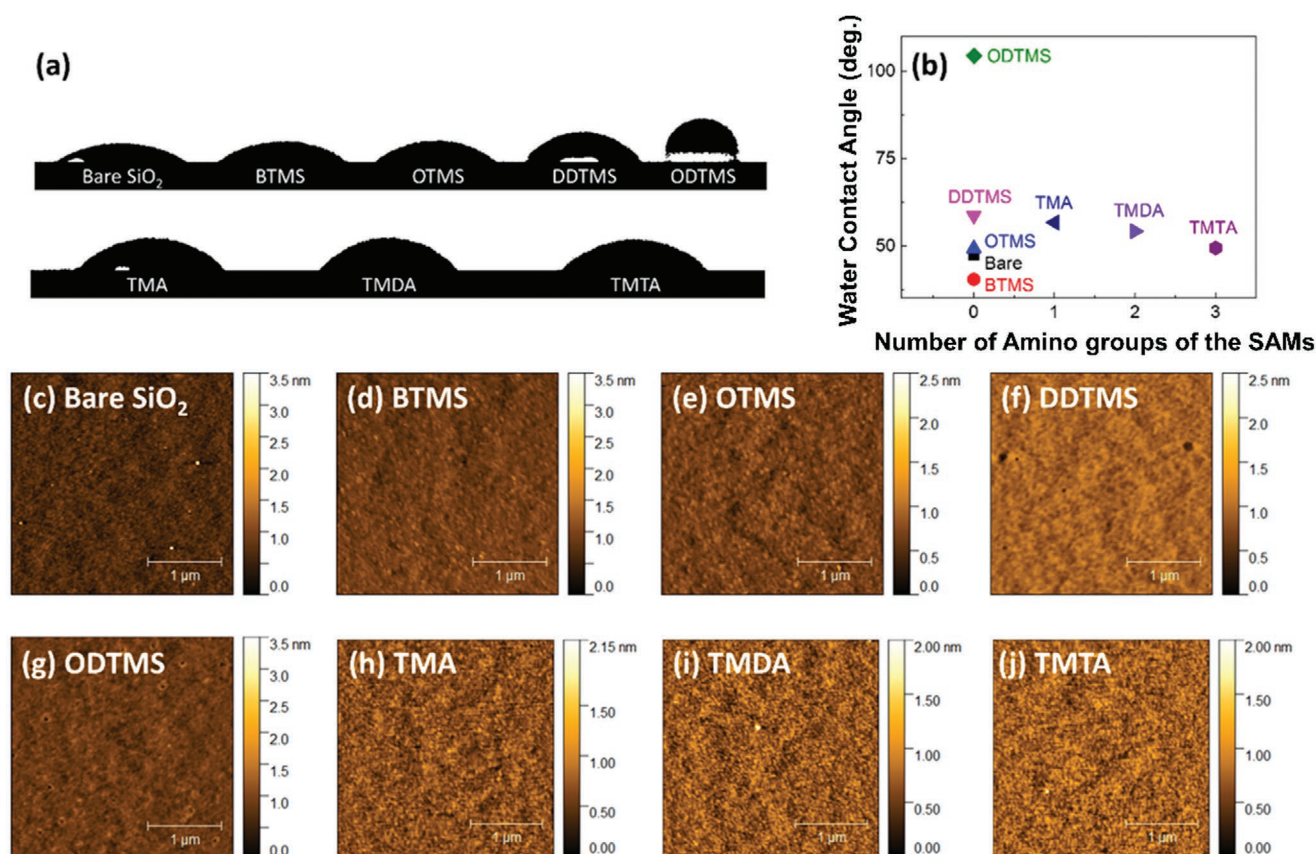

Figure 2. a) Photograph of a drop of distilled water on each SAM-treated SiO_2/Si substrate. b) Water contact angle of each SAM-treated surface with the number of amino groups in the SAMs. c–j) AFM topography of each SAM-treated SiO_2/Si substrates.

as the numbers of amino group of A-SAMs increase. It has to be pointed out that since all A-SAM-treated substrates are hydrophilic (water contact angle ≤ 60°) the absolute magnitude of the values is unreliable when obtained in air as here, but they can still provide a trend among the aminosilane materials. Not surprisingly, for A-SAM-treated surfaces, reported CPD values are very scarce and we are thus limited to a comparison of our values to those reported for slightly different A-SAM materials. The surface potential value of *N*-(6-aminohexyl)aminopropyltrimethoxysilane relative to ODTMS was −50 mV[41] and that of [3-(*N*,*N*′-dimethylamino) propyl]triethoxysilane (MAPS) was 1.04 V.[11] While the literature-reported CPD values unfortunately vary from paper to paper, the surface potential values listed above were reliably obtained from numerous samples and the resulting values are similar to the values reported for MAPS.[11]

2.2. OFET Characteristics: Relationship between OFET Mobility and Thin Film Morphology

Figure 3 depicts the electrical characteristics of OFETs fabricated with 25 nm thick PTCDI-C8 films on each SAM-treated substrate. As can be seen in I_d–V_g characteristics of OFETs (Figure 3a), the on-current values and the operating voltages (onset voltage, V_{on}, and a threshold voltage, V_{th}) vary significantly with the SAM materials that were used to treat the substrates. The discussion in this section focusses on the resulting carrier mobilities whereas the impact on the device voltage metrics is discussed in Section 2.3.

ODTMS, TMA, and TMDA-treated substrates were found to lead to improved PTCDI-C8 OFETs. Figure 3b shows the field-effect mobility of OFETs as a function of the number of amino groups on SAMs. The OFET mobility values for substrates treated with BTMS (0.042 $cm^2\ V^{-1}\ s^{-1}$), OTMS (0.013 $cm^2\ V^{-1}\ s^{-1}$), and DDTMS (0.014 $cm^2\ V^{-1}\ s^{-1}$) are similarly low, comparable to that of OFETs fabricated on bare SiO_2 substrate (0.048 $cm^2\ V^{-1}\ s^{-1}$). Of the C-SAM OFETs, only those fabricated on ODTMS-treated surfaces showed a significantly improved mobility (0.22 $cm^2\ V^{-1}\ s^{-1}$) compared to bare SiO_2 devices. A-SAM OFETs also exhibit higher carrier mobility values of 0.30, 0.17, and 0.12 $cm^2\ V^{-1}\ s^{-1}$ for devices fabricated on TMA, TMDA, and TMTA-treated substrate, respectively, all of which are higher than the mobility values measured for the C-SAM materials – with the exception of ODTMS.

As stated above, it is well established that modifications of the gate dielectric surface can induce differences in the morphology of OSC films which in turn can strongly influence the carrier mobility.[42–44] In particular, the morphology of the first layer of semiconductor films in the channel region near the dielectric interface is known to impact the carrier mobility.[1,18,22,24,45] The second layer is still significant since it can offer additional

© 2021 The Authors. Advanced Materials Interfaces published by Wiley-VCH GmbH

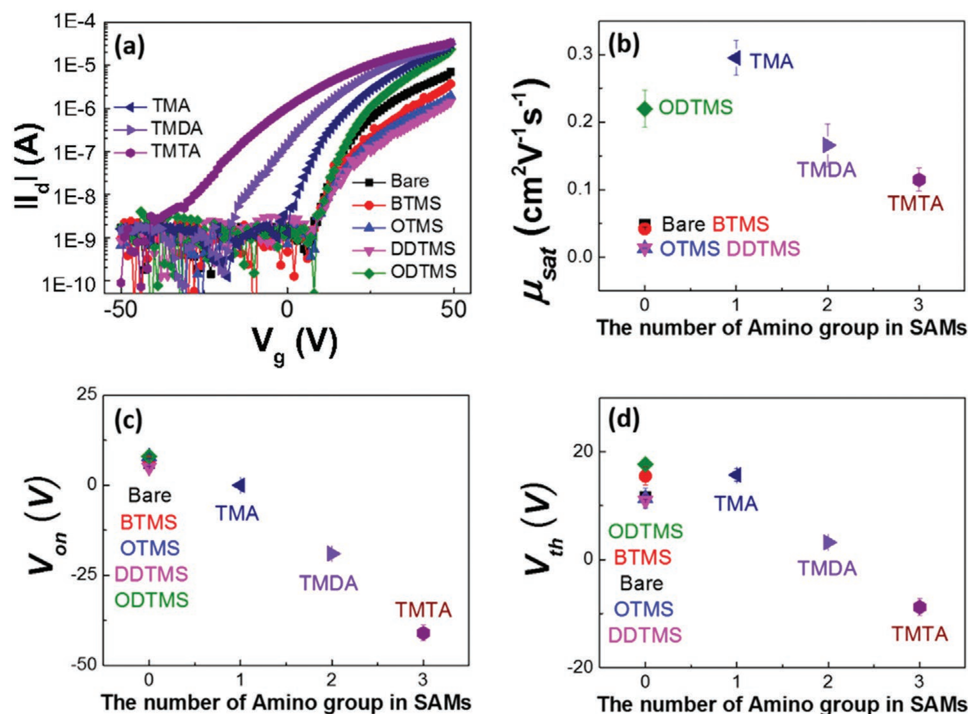

Figure 3. a) The I_d–V_g characteristics, b) the saturation mobility, c) the onset voltage, and d) the threshold voltage of OFETs fabricated with PTCDI-C8 films (25 nm thickness) deposited on each SAM-treated surface.

pathways for the charge carriers by bridging across the grain boundaries of the first layer.[1] In order to correlate the observed carrier mobility values with the film morphology, we thus analyzed the morphology of the first few layers in the PTCDI-C8 films on the different SAM surfaces. Since the thickness of a single monolayer of PTCDI-C8 film is known to be around 2 nm,[46] we fabricated PTCDI-C8 films with 2 and 5 nm thickness to obtain the first and second layer morphologies on the SAM-treated surfaces (We also obtained the thicker film morphology but as can be seen Figures S2 and S3, Supporting Information it was difficult to observe any morphological differences among the films with thickness of 25 and 10 nm.).

AFM topography of the resulting films is provided in **Figure 4** for 2 nm-thick films and **Figure 5** for 5 nm-thick films. As shown in Figure 3, the mobility value of A-SAM-treated oxides and ODTMS-treated oxides is over 2.5× higher than that of the rest. We think that the main reason for similarly low mobility values in OFETs fabricated on BTMS, OTMS, and DDTMS-treated surfaces and bare SiO_2 substrate might be the rather poor grain connectivity within the first layer, that is, the

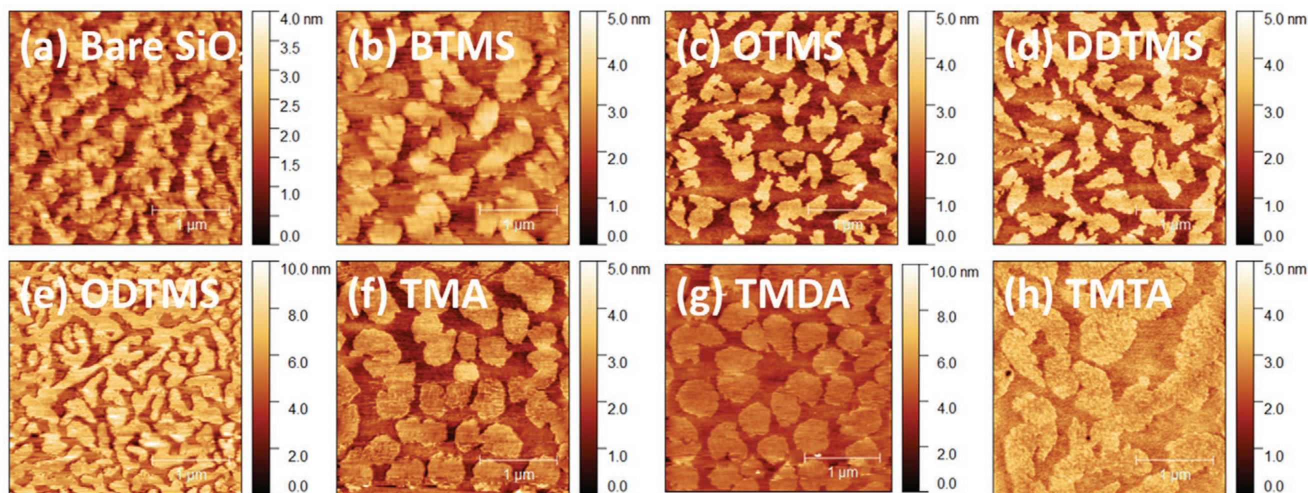

Figure 4. AFM topography of PTCDI-C8 films with 2 nm thickness on a) the bare SiO_2/Si substrate and the substrates treated with b) BTMS, c) OTMS, d) DDTMS, e) ODTMS, f) TMA, g) TMDA, and h) TMTA.

© 2021 The Authors. Advanced Materials Interfaces published by Wiley-VCH GmbH

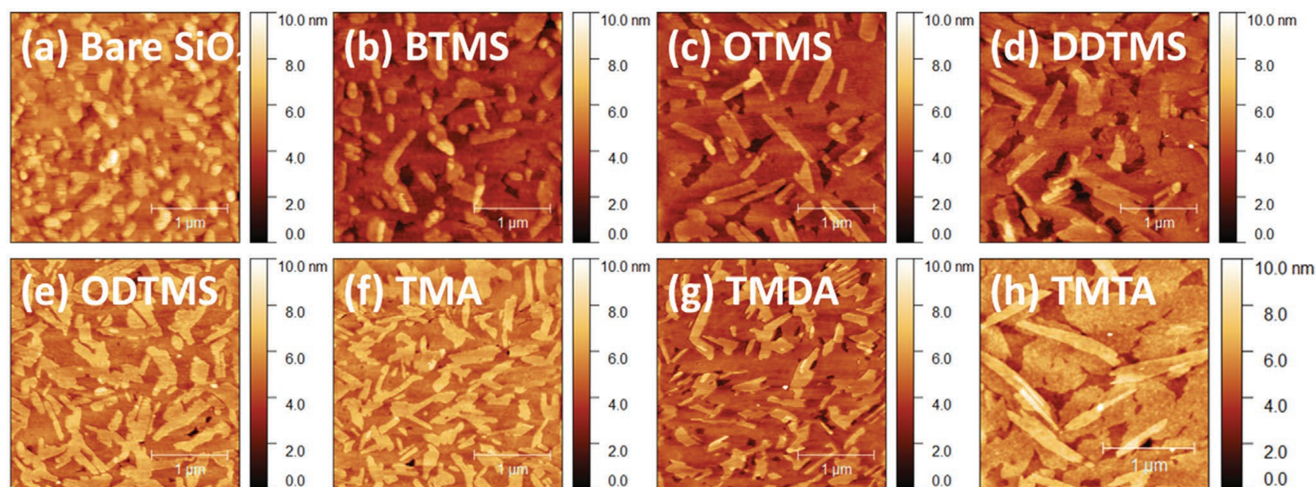

Figure 5. AFM topography of PTCDI-C8 films with 5 nm thickness on a) the bare SiO_2/Si substrate and the substrates treated with b) BTMS, c) OTMS, d) DDTMS, e) ODTMS, f) TMA, g) TMDA, and h) TMTA.

coverage of the first layer is still low even when a nominal amount of two monolayers worth of material has been deposited (Figures 4a–d and 5a–d). On the other hand, the electrical mobility of OFETs fabricated on ODTMS-treated surfaces (0.22 $cm^2 V^{-1} s^{-1}$) is significantly higher, which is likely due to the high interconnectivity of grains at the first layer and the well-covered film morphology by the second layer as shown in Figures 4e and 5e. Furthermore, previous reports suggested that the grain shape of the first layer could be also relevant to the resulting OFET mobility values.[17,22] A first layer with circular shaped grains usually resulted in high performances of pentacene transistors. In our case, the A-SAM-treated substrates with more round PTCDI-C8 grains also produce a better OFET performance than the C-SAM-treated substrates with comparable water contact angle – ODTMS films are the exception as they have a different water contact angle than all other SAM materials and as already discussed lead to more wetting of the PTCDI-C8 films with well interconnected grains already at 2 nm film thickness.

An interesting finding is that the morphologies of the 2 nm thick films and their 5 nm thick counterparts differ greatly in some cases. For example, the 2 nm morphologies that belong to the best OFETs (in terms of the carrier mobility), namely the ODTMS-treated and TMA-treated devices, are quite different, with well interconnected elongated grains in the ODTMS case and large circular islands in the TMA case (Figure 4e,f). Nonetheless, the morphology of the corresponding 5 nm thick PTCDI-C8 films is nearly indistinguishable (Figure 5e,f). Since both the 2 and 5 nm thick films represent snapshots of the evolution of the first and second layer morphology that are most relevant to electrical transport in OFETs,[21] this striking difference shows how complex the growth is and how challenging it is to link morphology to device performance. The 5 nm film morphology could actually explain why among all fabricated OFETs the ones made on TMA and ODTMS-treated surfaces show the first and second highest electrical mobility (0.30 and 0.22 $cm^2 V^{-1} s^{-1}$). In both cases, the film coverage appears near complete with the second layer's grains and far fewer vacancies (first layer holes) in these films (Figure 5e,f) than are visible in the 5 nm films on the other C-SAM and A-SAM-treated substrates.

Finally, the trend of decreasing mobility with increasing lengths of alkyl chain and numbers of amino groups in the A-SAM materials can also be rationalized by the AFM data. The 5 nm thick PTCDI-C8 films on TMDA and TMTA-treated substrates have more visible film holes/vacancies than the films on TMA-treated substrates (Figure 5e–h). This morphological difference might be related to the different surface roughness (TMA < TMDA < TMTA) that we had observed in the A-SAM-treated substrates but also the degree of interaction between the OSC molecules and the amino groups on the SAM molecule that change with the number of amino groups. In addition, Figures S4a–h and S4i–p, Supporting Information depict the AFM images and the associated line cut profiles of the first PTCDI-C8 layer, respectively. The surface profiles of films on A-SAM-treated surfaces are shown in Figure S4n–p, Supporting Information. With an increasing number of amino groups (from TMA to TMTA) in the A-SAMs, the surface roughness of the first OSC layer significantly increases while the profiles of surfaces for the other SAM substrates look similar.

2.3. A-SAM-Induced Threshold and Onset Voltage Shifts

One of the findings from the OFET data presented in Figure 3 was that, besides the mobility, the on-set voltage V_{on} and threshold voltage V_{th} also show a significant dependence on the A-SAM material that was used to treat the gate oxide (Table S1, Supporting Information). While the V_{on} can be useful to estimate interfacial trap densities (see Supporting information), shifts in the threshold voltage are not only technologically highly important but also particularly interesting to discuss since they can be directly related to changes in the free carrier densities in the channel, that is, doping effects. Therefore, in this section we want to discuss the impact of the various SAM-treated dielectrics on the threshold voltage and elucidate the origin behind the observed A-SAM material dependent threshold voltage shifts.

© 2021 The Authors. Advanced Materials Interfaces published by Wiley-VCH GmbH

In this work, the KPFM-determined surface potentials were negligible compared to the measured threshold voltage differences (Figures S1c, S9, Supporting Information, Figure 3d). The threshold voltage values of the C-SAM OFETs were all small and similar, whereas the threshold voltages of the A-SAM OFETs were found to be strongly shifted, with the magnitude of the shift increasing with the number of amino groups on A-SAMs. This finding points to the threshold voltage shifts being caused by the interface between the A-SAM films and the PTCDI-C8 films and is consistent with Aghamohammadi et al. who found that for strongly electronegative fluorinated SAMs the threshold voltage shift is much larger than the surface potential induced by the SAM dipole moment whereas for C-SAMs this approximation is roughly valid.[38]

Figure 3d plots the threshold voltage of OFETs fabricated on each SAM-treated surface. We find that the threshold voltage is not clearly correlated to the film morphology as the mobility[2,28] but in our case seems to depend on the number of amino groups of A-SAMs. In order to address this question, we firstly test the hypothesis of dipole-induced accumulation charges and analyze the dipole moments of the SAMs using density functional theory (DFT)-based approaches (see section 4). All SAMs were simulated with a trimethoxysilane group attached to the alkyl chains and show a dipole moment that is directed towards the substrate (**Table 1**). For the C-SAMs, the alkyl chain does not exhibit considerable excess charges. This leads to dipole moments of +2.8 D quite independently of chain length. In contrast, A-SAMs show a variation in the dipole moments with increasing distance between the terminal amino group and the trimethoxysilane group (cf. Table 1). However, the variation in the dipole moment is relatively small between the different A-SAMs and the dipole moment of TMA is of comparable size as the one by the C-SAMs leading us to the conclusion that this effect cannot dominantly cause the observed differences in the threshold and onset voltages.

In addition to the electrostatic characteristics of the neutral SAMs, the amino group of A-SAM-treated substrates is also well known for being susceptible to protonation on SiO_2 or glass substrates,[40,47] which needs to be considered as well. X-ray photoelectron spectroscopy (XPS) was performed to quantify the degree of protonation in the A-SAMs (Figure S6, Supporting Information). We found that neutral (NH, NH_2, at 400 eV) and protonated amino species (NH_2^+, NH_3^+, at 402 eV) coexist in all the A-SAM-treated surfaces but at different ratios: The ratio of protonated:neutral amino groups was 30:70, 20:80, and 10:90 for TMA, TMDA, and TMTA, respectively, in agreement with a previous report.[47] However, if the different A-SAM molecules grow at a similar density on the substrate and if one considers the different numbers of amino groups on them (of which only the amino group nearest to the substrate would be protonated), the total number of SAM molecules in each of the A-SAM films that carry a protonated amino group is in fact similar: Based on the above measured ratios between protonated and neutral amino groups, about every third A-SAM molecule carries a protonated amino group.

Table 1. Simulated dipole moments of the neutral and protonated SAMs in D. Positive (negative) values represent a dipole moment pointing towards the organic film (substrate).

Dipole moment (*D*)	OTMS	ODTMS	TMA	DMTMA	TMDA	TMTA
Non-protonated form	−1.9	−1.9	−1.7	−1.8	−2.8	−3.3
Protonated form	–	–	+15.4	+13.4	+10.8	+5.7

Consequently, the dipole moments of the protonated A-SAMs essentially affect the energy landscape. Based on DFT calculations, we find that protonation is energetically most favorable at the amino group that is closest to the trimethoxysilane group as shown in Figure S7 and Table S1, Supporting Information, which is in agreement with a previous XPS study.[47] Considering this aspect, the dipole moments of the protonated A-SAMs were calculated. These molecules exhibit a flipped dipole moment pointing towards the organic film (i.e., −1.7 D for the non-protonated TMA and +15.4 D for the protonated TMA, Table 1) in accordance with previous studies.[11,37,40] Also, the dipole moment value decreases with increasing the alkyl chain length of the terminating group on A-SAMs, +15.4, +10.8, and +5.7 D for the protonated TMA, TMDA, and TMTA, respectively. Combining this observation with the approximately equal density of the protonated molecules for all three A-SAMs, the strongest threshold voltage shift should occur for TMA and the smallest one for TMTA, which is in stark contrast to the experimental findings.

To be able to confidently rule out the dipole moments as origin behind the observed trends and for further insights in the underlying effects, we add an additional A-SAM material to the analysis of the threshold and onset voltage shifts. 3-(*N*, *N′*-dimethylamino)propyl]trimethoxysilane (DMTMA) has a similar molecular structure to TMA (Figure S7, Supporting Information): Both have a single amino group and only differ structurally by DMTMA having two methyl groups terminating the amino group where TMA has hydrogens. Because of this structural difference, the dipole moments of DMTMA and TMA are quite different in both the non-protonated and protonated cases (Table 1). On the other hand, OFETs that were fabricated on DMTMA-treated oxides show an average threshold voltage of 12.55 V, only slightly smaller than that of the OFETs made on the TMA-treated oxides. Based on these findings, the variation in dipole moment can be excluded as an explanation for the experimentally observed trend in the threshold voltage shift of OFETs.

As already stated, another hypothesis to explain the threshold voltage shift would be a possible charge transfer from the A-SAM molecules to the PTCDI-C8 molecules. Kobayashi et al. had already suggested "weak electron transfer" from the lone electron pairs on the amino group of an A-SAM molecule to the semiconductor might take place, but this has so far remained speculation.[37] To analyze this effect in more detail, we created model structures consisting of an A-SAM molecule and a PTCDI-C8 molecule as depicted in **Figure 6**a. The Hirshfeld atomic charges are calculated for these structure complexes for the protonated and the non-protonated A-SAMs, while assuming overall charge neutrality for the complex (see also Figures S10–S17, Supporting Information). While both molecules in the complex are almost neutral for the non-protonated A-SAMs, an intermolecular charge transfer configuration is observed for all protonated A-SAMs with the PTCDI-C8 molecule being negatively charged by almost an electron

© 2021 The Authors. Advanced Materials Interfaces published by Wiley-VCH GmbH

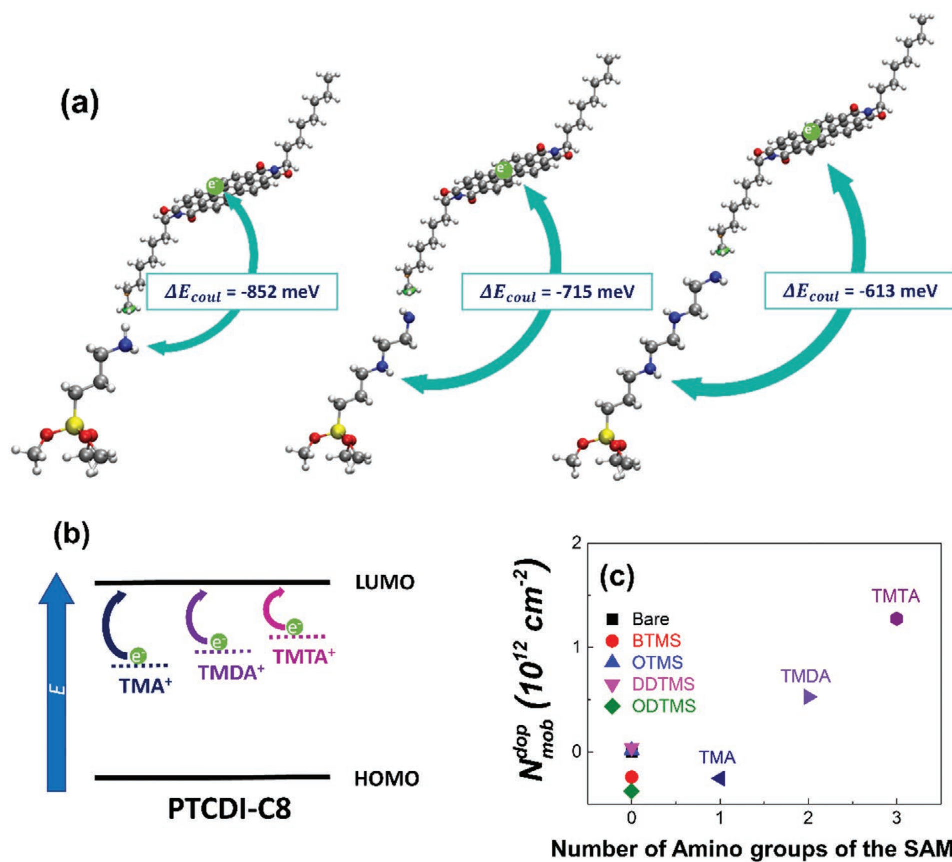

Figure 6. a) Coulombic binding energy difference between the transferred electron and the protonated amino group of TMA, TMDA, and TMTA. b) Schematic energy diagram of the relation between SAM-induced mobile carrier and PTCDI-C8. c) The mobile carrier density induced by SAMs of OFETs fabricated on each SAM-treated surfaces estimated from Equation (1).

(0.7 *e* or more). This result is very surprising because the simulations are performed in vacuum where no dielectric environment stabilizes the charge transfer dipole. In the actual devices, the polarization by the surrounding molecules would even more favor the occurrence of intermolecular electron transfer configurations consisting of the protonated SAMs and the negatively charged organic film. This leads us to the conclusion that the protonated amine induces charge accumulation in the OSC film (at overall charge neutrality) but in absence of significant electron transfer from the amine lone pair.

Another surprising result from the calculations is the fact that the electron transfer appears to be independent of the length of the A-SAM and the distance of the protonated amino group from the PTCDI-C8 molecule. In addition, even calculations performed for TMDA and TMTA with protonation of more than one amino group show only single-electron charge transfer from an analysis of the Hirshfeld charges in these cases.

Energetically it is important though that with the varying alkyl chain length of the A-SAMs, the distance between the negatively charged PTCDI-C8 molecule and the protonated amino group also varies.[48] The corresponding Coulomb binding energy (ΔE_{coul}) between the transferred electron and the protonated amino group in a single SAM-PTCDI-C8 dimer decreases from –852 meV for TMA to –613 meV for TMTA (Table S1, Supporting Information). Consequently, the transferred electrons are less strongly bound for TMTA than for TMA. We also performed the calculations for DMTMA since it is structurally similar to TMA and can demonstrate the relevance of the observed effects. The Coulomb binding energy of –800 meV between protonated DMTMA and PTCDI-C8 is slightly smaller than the value of protonated TMA (Figure S7 and Table S1, Supporting Information). This effect is related to the extra methyl groups on DMTMA that extend the vertical length of the molecule above the protonated amino group. The threshold voltage of devices fabricated on the DMTMA-treated oxides was accordingly slightly smaller than that of TMA-treated oxides (12.55 V for DMTMA and 15.69 V for TMA). This demonstrates that small structural manipulation of the A-SAM affects the threshold voltage shift.

The most important result from the calculations is that the binding energy systematically varies with the length of the A-SAM molecule (more precisely the length of the molecular section above the protonated bottom amino group), leading to the generation of varying densities of mobile charges in the OSC. While these binding energies of an isolated pair of electron on PTCDI-C8 and protonated amino group on an A-SAM molecule significantly exceed $k_{\mathrm{B}}T$, the fact that there are many of such pairs in the film (about every third A-SAM molecule produces such a pair) explains why the electrons transferred from the protonated A-SAM to the PTCDI-C8 are mobile charges and thus produce a threshold voltage shift in the devices. **Figure 7**

© 2021 The Authors. Advanced Materials Interfaces published by Wiley-VCH GmbH

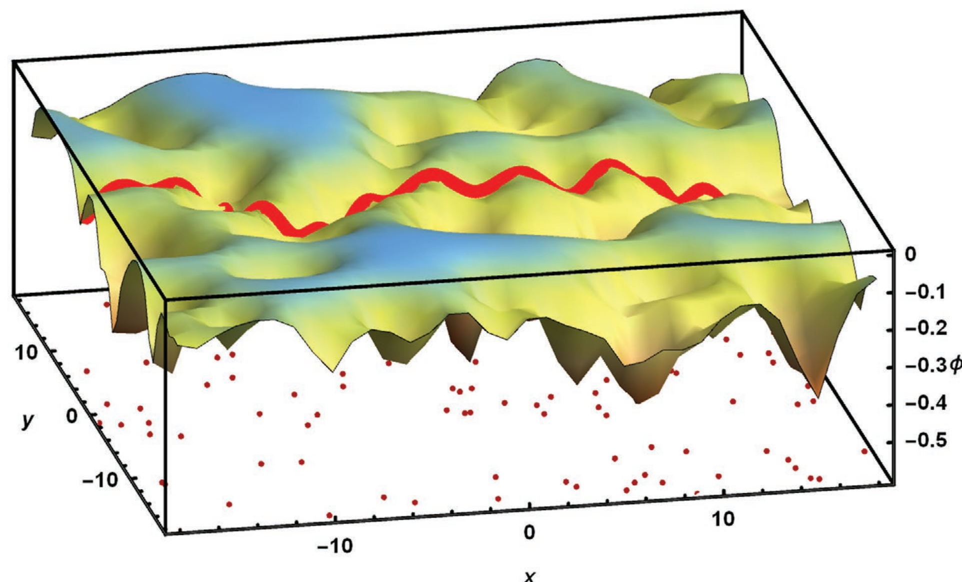

Figure 7. Illustration of carrier motion in the PTCDI-C8 OFET device's transport channel under presence of many charged dopants. For this schematic, the electrostatic potential Φ [eV] is caused by randomly placed dopant impurities with about 30% doping ratio which corresponds to the protonation ratio we find in the A-SAMs. The lateral positions are indicated as dots. The red line indicates the charge's trajectory. The resulting activation barriers for individual hops between local minima in the lateral channel direction are below 0.1 eV, even when the actual electron–hole pair Coulomb binding energy is ≈1.4 eV.

shows the effect of the quenching of the individual pair Coulomb energy in the presence of many neighboring pairs. When we randomly place electrons and positive charges at a spatial density of 30%, there are electron trajectories along which the site-to-site hopping barrier is <0.1 eV. Therefore, individual Coulomb barriers of several hundred meV overlap and are reduced to effectively only tens of meV.[49,50] Overall, the theoretical results readily explain why with a decreasing distance of the protonated amino group and the PTCDI-C8 layer we observe an increasing doping effect.[48] The SAM-induced mobile charges are added to the interface (Figure 6b) and can accumulate and contribute to the channel charges, causing the threshold voltage (the minimum required voltage to form a complete accumulation channel) to be shifted.[28] The hypothesis that the shift in the threshold voltage is indeed related to the distance between the protonated amino group of the A-SAMs and the PTCDI-C8 layer and thus the length of the alkyl chain above the bottom protonated amino group was even further corroborated by recent test devices fabricated on the SiO_2/Si substrates treated with the two additional A-SAM materials: *3*-(Triethoxysilyl)propylamine (TEA) and *N*-[3-(triethoxysilyl) propyl]ethane-1,2-diamine (TEDA) have a triethoxysilane group and contain the same number of amino groups as TMA and TMDA, respectively (Figure S8a and b). The OFETs fabricated on the substrates treated by A-SAMs with the same number of amino group resulted in similar I_d-V_g characteristics and onset and threshold voltages as depicted in Figure S8c–e, Supporting Information. All these findings demonstrate that the threshold voltage shift is related to the length of the alkyl chain above the protonated amino group of the A-SAMs.

Finally, the number of additional mobile carriers induced by a SAM on the dielectric surface can be estimated by Equation (1) (for details see Supporting information) where ΔV_{th} is the threshold voltage shift between undoped and doped devices, C_{ox} is the gate capacitance of SiO_2 per unit area (10 nF cm^{-2}), and e is the elementary charge.[51]

$$N_{mob}^{dop} = \Delta V_{th} C_{ox} / e \quad (1)$$

The density of the so-calculated additional mobile carriers (Figure 6c and **Table 2**) relative to the bare SiO_2 substrate samples increases, as expected, with increasing lengths of the alkyl chain of the A-SAMs: -2.54×10^{11} cm^{-2} (the value < 0 means that the number of mobile carriers has slightly decreased relative to the bare Si substrate), 5.27×10^{11}, and 1.28×10^{12} cm^{-2}.

Table 2. The mobile carrier density induced by SAMs of OFETs fabricated on each SAM-treated surfaces estimated from Equation (1). Note that negative values in N_{mob}^{dop} mean a reduction in free carriers relative to the bare Si substrate samples (e.g., due to the introduction of deep trap states), positive numbers show a doping effect.

	Bare	BTMS	OTMS	DDTMS	ODTMS	TMA	TMDA	TMTA
ΔV_{th} [V]	0	3.86	−0.28	−0.66	6.03	4.07	−8.44	−20.44
N_{mob}^{dop} [10^{12} cm^{-2}]	0.00	−0.24	0.02	0.04	−0.38	−0.25	0.53	1.28

© 2021 The Authors. Advanced Materials Interfaces published by Wiley-VCH GmbH

3. Conclusion

From a device fabrication point of view, we successfully enhanced the electrical performance metrics of OFETs based on n-type polycrystalline semiconductors through the modification of the gate oxide with SAMs, from C-SAMs to A-SAMs. Among the tested SAM materials, TMA and TMDA treatment of the gate oxide was found to be the most suitable for operation by lower voltages with high carrier mobility. Overall, the mobility of OFETs fabricated on A-SAM-treated surfaces was significantly higher than that of OFETs fabricated on C-SAM treated surfaces, with the exception of ODTMS.

As an in our opinion much more important result, this study for the first time sheds light on the nature of the doping effect that occurs when the gate oxide is treated with polar aminosilane materials. Specifically, we were able to explain how the observed and desirable doping effect which resulted in a control of the threshold voltage towards zero volt, systematically varied with the length of the analyzed A-SAM materials. Based on a combination of XPS measurements and theoretical modeling we identified that most likely scenario as: per protonated amino group—which occurs on about every third A-SAM molecule in the SAM on the dielectric—one mobile electron is stabilized in the OSC film, leading to the observed doping effect. In contrast, the non-protonated A-SAM molecules, while being the doping agent, do not provide directly an electron to the organic film by ionization to its cationic form, as observed for other n-dopants.[48]

The dipole moments of the polar A-SAM molecules could on the other hand not explain the observed threshold voltage shift. Theoretical calculations showed that protonation of the bottom-most amino group (in a situation where A-SAM molecules grow with their silane group down on a substrate) is energetically most favorable. The number of additional doped channel charges in the device then depends on the transferred electron's Coulomb binding energy to the protonated amino group (since its motion is then thermally activated) which in turn directly depends on the length of the molecular section above the bottom-most, protonated amino group. We could also show that in dense SAM layers, the activation energy is on the order of $k_B T$. We are confident that this finding should also help settle the ongoing discussion in literature on the nature and origin of threshold voltage shifts as observed for OFETs with similar polar SAM gate dielectric treatments.[35,38] Since the degree of the threshold voltage shift appears to depend on the length of the molecular section above the bottom-most amino group, this is also a synthetic design rule to tune the doping activity of such materials.

Finally, even though TMTA-treated substrates produce large shifts in threshold voltage of PTCDI-C8 OFETs by supplying more mobile carriers, the field-effect mobility was the highest (by a slight margin) when using TMA-treated substrates. Therefore, to optimize OFET performances through modification of the gate oxide by SAMs with functional groups both the OSC film growth kinetics and the interaction between the OSC and the functional groups of the SAMs should be considered.

Overall, this study suggests A-SAM-treated gate oxide could be applied for other n-channel devices as well to achieve high n-type electrical performances. Furthermore, new A-SAM molecules could be designed to utilize the findings from this study – stable charge transfer from the closest amino group to the anchor group with growth-promoting terminal functional groups.

4. Experimental Section

Surface Treatment of SAMs on the Gate Oxide: Heavily doped Si wafers passivated with 300 nm SiO_2 layer were cleaned with ultrasonication in acetone and isopropanol for 10 min and subsequent UV-ozone exposure for 20 min each. The solution of each SAM with a concentration of 3×10^{-3} M in trichloroethylene was spin-coated at 3000 rpm on the SiO_2/Si substrates. The used C-SAMs are as follows; butyltrimethoxysilane (BTMS, purchased from abcr GmbH), octyltrimethoxysilane (OTMS, purchased from Sigma-Aldrich), dodecyltrimethoxysilane (DDTMS, purchased from Alfa Aesar), and octadecyltrimethoxysilane (ODTMS, purchased from Sigma-Aldrich). The used A-SAMs are as follows; 3-(trimethoxysilyl) propylamine (TMA, purchased from Gelest), *N*-[3-(trimethoxysilyl) propyl]ethylenediamine (TMDA, purchased from Sigma-Aldrich), N^1-[3-(trimethoxysilyl)propyl]diethylenetriamine (TMTA, purchased from Sigma-Aldrich), 3-(triethoxysilyl)propylamine (TEA, purchased from Sigma-Aldrich), *N*-[3-(triethoxysilyl)propyl)ethane-1,2-diamine) (TEDA, purchased from Sigma-Aldrich). The SAM-treated wafers were placed together with a small vial of ammonium hydroxide in a evacuated desiccator at 5 mbar condition for 15 h with the ammonium hydroxide vapor promoting the SAM crosslinking.[26] The SAM-treated substrates were then cleaned with water and toluene and dried with nitrogen and annealed on a hotplate at the temperature of 120 °C for 10 min.

Device Fabrication: On the SAM-treated substrates, 25 nm of PTCDI-C8 (Sigma-Aldrich, sublimed) was thermally evaporated at the substrate temperature of 120 °C and a rate of 0.2–0.5 Å s^{-1} with the OSC crucible temperature of 170 °C under high vacuum condition (10^{-7} mbar). Afterwards, 50 nm thick gold source/drain top electrodes were evaporated with a shadow mask under high vacuum condition (10^{-7} mbar) on PTCDI-C8 films. The channel width and length of all devices were 1000 and 100 µm, respectively.

Characterization and Measurement: Atomic force microscopy (AFM) was performed with a Nanosurf Flex-Axiom with C3000 controller. The silicon AFM tips (Tap190Al-G, purchased from Budget Sensors) with an aluminum reflective coating were used in tapping mode. Kelvin probe force microscopy (KPFM) data was obtained with applying 2 V in ambient conditions by the Flex-Axiom AFM in non-contact mode. The gold conductive tips, ElectriMulti75-G, were purchased from Budget Sensors. The KPFM sample was prepared as Au/SAMs/SiO_2/Si layer stack. On each SAM-treated SiO_2/Si wafer surfaces, 50 nm thick gold source/drain electrodes were evaporated with a shadow mask under high vacuum condition (10–7 mbar). The resulting CPD (V_{CPD}) between a tip and a sample is defined as $V_{CPD} = (\varphi_{tip} - \varphi_{sample})/(-e)$.[52] All the AFM and KPFM images were processed and analyzed with the software "*Gwyddion* version 2.50". The water contact angles were obtained with very small droplets (≈4 µL) of distilled water on SAM-treated surfaces from magnifying photographs taken with a Nikon COOLPIX P610. The contact angle itself was obtained from the "ImageJ vers.1.51j8" software developed by Wayne Rasband with the contact angle plugin. All current-voltage characterizations of devices were carried out by two connected Keithley 236 source meters in a nitrogen-filled glove box using the software SweepMe! (sweep-me.net). The field-effect mobility values were extracted using Equation (2) by performing a linear fit to $\sqrt{I_d}(V_g)$ in the saturation transfer curves with an applied drain voltage of 50 V. Here, L is the channel length, W is the channel width and C_i is the capacitance of the gate dielectric per unit area (SiO_2 = 10 nF cm^{-2}).

$$\mu = 2L/WC_i\left[\sqrt{I_d}/\left(V_g - V_{th}\right)\right]^2 \tag{2}$$

The threshold voltage values were extracted from the saturation transfer curves of each device, obtained from the linear fit to $\sqrt{I_d}(V_g)$ as its intercept with the V_g axis.

© 2021 The Authors. Advanced Materials Interfaces published by Wiley-VCH GmbH

Theoretical Calculations of Molecular Dipoles and Coulombic Binding Energy: Density functional theory (DFT)-based calculations were performed to analyze the electrostatic characteristics of the SAMs as well as charge transfer between the SAMs and the PTCDI-C8 molecules.

The geometry optimization of single SAM molecules was performed using the NWchem software package in combination with the long-range corrected CAM-B3LYP exchange correlation functional and the cc-pVTZ basis set.[53–58] Dipole moments were calculated for the neutral and protonated A-SAMs (cationic) at the position of the Si atom.

To identify whether charge transfer occurs between A-SAMs and PTCDI-C8, comparable molecular model complexes were created with PTCDI-C8's alkyl chains directed towards the A-SAM molecule as depicted in Figure 6. The subsequent geometry optimization of the complexes was carried out at the CAM-B3LYP/3-21G level of theory including empirical van der Waals corrections.[59,60] Charge transfer was evaluated based on the atomic charges of the complex using the Hirshfeld charge approach as implemented in the Gaussian09 suite at the CAM-B3LYP/cc-pVTZ level of theory.[61–64] The Coulombic binding energy difference (ΔE_{coul}) was calculated with the relaxed geometries of the complexes using the atomic Hirshfeld charges of the separated relaxed molecules in gas phase q_i^D and q_j^A with Equations (3) and (4).[65]

$$E_{\text{coul}} = \frac{1}{4\pi\varepsilon_0}\sum_{i,j}\frac{q_i^D q_j^A}{\left|\boldsymbol{R}_i^D - \boldsymbol{R}_j^A\right|} \tag{3}$$

$$\Delta E_{\text{coul}} = E_{\text{coul}}(\text{A-SAM}^+,\ \text{PTCDI}^-) - E_{\text{coul}}(\text{A-SAM, PTCDI}) \tag{4}$$

Supporting Information

Supporting Information is available from the Wiley Online Library or from the author.

Acknowledgements

The authors would like to acknowledge support by the German Excellence Initiative via the Cluster of Excellence EXC 1056 "Center for Advancing Electronics Dresden (cfaed)". This work was supported by an Inspire grant from the Center for Advancing Electronics and the program IPID4all by the DAAD and the Graduate Academy of TU Dresden. F.O. acknowledges the Deutsche Forschungsgemeinschaft (grant OR 349/1) for financial support.

Open access funding enabled and organized by Projekt DEAL.

Conflict of Interest

The authors declare no conflict of interest.

Data Availability Statement

Research data are not shared.

Keywords

aminosilanes, charge transfer, gate oxide modification, organic field-effect transistors, PTCDI-C8 morphology

Received: February 27, 2021
Revised: June 3, 2021
Published online: July 26, 2021

[1] S. Y. Yang, K. Shin, C. E. Park, *Adv. Funct. Mater.* **2005**, *15*, 1806.
[2] C. Celle, C. Suspène, M. Ternisien, S. Lenfant, D. Guérin, K. Smaali, K. Lmimouni, J. P. Simonato, D. Vuillaume, *Org. Electron.* **2014**, *15*, 729.
[3] T. Minari, M. Kano, T. Miyadera, S.-D. Wang, Y. Aoyagi, K. Tsukagoshi, *Appl. Phys. Lett.* **2009**, *94*, 093307.
[4] U. Zschieschang, M. Halik, H. Klauk, *Langmuir* **2008**, *24*, 1665.
[5] P. Saravanan, K. Jayamoorthy, S. Anandakumar, *J. Lumin.* **2016**, *178*, 241.
[6] T. Mosciatti, P. Greco, T. Leydecker, M. Eredia, F. Biscarini, P. Samorì, *ACS Omega* **2017**, *2*, 3502.
[7] M. F. Calhoun, J. Sanchez, D. Olaya, M. E. Gershenson, V. Podzorov, *Nat. Mater.* **2008**, *7*, 84.
[8] C. Y. Kao, B. Lee, L. S. Wielunski, M. Heeney, I. McCulloch, E. Garfunkel, L. C. Feldman, V. Podzorov, *Adv. Funct. Mater.* **2009**, *19*, 1906.
[9] N. Shin, J. Zessin, M. H. Lee, M. Hambsch, S. C. B. Mannsfeld, *Adv. Funct. Mater.* **2018**, *28*, 1802265.
[10] H. Chen, X. Guo, *Small* **2013**, *9*, 1144.
[11] M. Nakano, I. Osaka, K. Takimiya, *Adv. Mater.* **2016**, *29*, 1602893.
[12] D. H. Kim, H. S. Lee, H. Yang, L. Yang, K. Cho, *Adv. Funct. Mater.* **2008**, *18*, 1363.
[13] F. Zhang, E. Mohammadi, X. Luo, J. Strzalka, J. Mei, Y. Diao, *Langmuir* **2018**, *34*, 1109.
[14] S. E. Fritz, T. W. Kelley, C. D. Frisbie, *J. Phys. Chem. B* **2005**, *109*, 10574.
[15] S. Steudel, S. De Vusser, S. De Jonge, D. Janssen, S. Verlaak, J. Genoe, P. Heremans, *Appl. Phys. Lett.* **2004**, *85*, 4400.
[16] W. H. Lee, J. H. Cho, K. Cho, *J. Mater. Chem.* **2010**, *20*, 2549.
[17] A. A. Virkar, S. Mannsfeld, Z. Bao, N. Stingelin, *Adv. Mater.* **2010**, *22*, 3857.
[18] Y. Hu, Q. Qi, C. Jiang, *Appl. Phys. Lett.* **2010**, *96*, 133311.
[19] M. J. Loiacono, E. L. Granstrom, C. D. Frisbie, *J. Phys. Chem. B* **1998**, *102*, 1679.
[20] M. Hambsch, T. Erdmann, A. R. Chew, S. Bernstorff, A. Salleo, A. Kiriy, B. Voit, S. C. B. Mannsfeld, *J. Mater. Chem. C* **2019**, *7*, 3665.
[21] F. Dinelli, M. Murgia, P. Levy, M. Cavallini, F. Biscarini, D. M. de Leeuw, *Phys. Rev. Lett.* **2004**, *92*, 116802.
[22] A. Virkar, S. Mannsfeld, J. H. Oh, M. F. Toney, Y. H. Tan, G. Liu, J. C. Scott, R. Miller, Z. Bao, *Adv. Funct. Mater.* **2009**, *19*, 1962.
[23] T. Umeda, D. Kumaki, S. Tokito, *J. Appl. Phys.* **2009**, *105*, 024516.
[24] H. Yang, T. J. Shin, M.-M. Ling, K. Cho, C. Y. Ryu, Z. Bao, *J. Am. Chem. Soc.* **2005**, *127*, 11542.
[25] M. L. Tang, T. Okamoto, Z. Bao, *J. Am. Chem. Soc.* **2006**, *128*, 16002.
[26] Y. Ito, A. A. Virkar, S. Mannsfeld, J. H. Oh, M. Toney, J. Locklin, Z. Bao, *J. Am. Chem. Soc.* **2009**, *131*, 9396.
[27] C. Goldmann, C. Krellner, K. P. Pernstich, S. Haas, D. J. Gundlach, B. Batlogg, *J. Appl. Phys.* **2006**, *99*, 034507.
[28] K. P. Pernstich, S. Haas, D. Oberhoff, C. Goldmann, D. J. Gundlach, B. Batlogg, A. N. Rashid, G. Schitter, *J. Appl. Phys.* **2004**, *96*, 6431.
[29] H.-I. Un, Y.-Q. Zheng, K. Shi, J.-Y. Wang, J. Pei, *Adv. Funct. Mater.* **2017**, *27*, 1605058.
[30] D. J. Gundlach, Y. Y. Lin, T. N. Jackson, S. F. Nelson, D. G. Schlom, *IEEE Electron Device Lett.* **1997**, *18*, 87.
[31] Y. Lin, D. Gundlach, S. Nelson, T. Jackson, *IEEE Electron Device Lett.* **1997**, *18*, 606.
[32] D. Shukla, S. F. Nelson, D. C. Freeman, M. Rajeswaran, W. G. Ahearn, D. M. Meyer, J. T. Carey, *Chem. Mater.* **2008**, *20*, 7486.
[33] Y. Jang, J. H. Cho, D. H. Kim, Y. D. Park, M. Hwang, K. Cho, *Appl. Phys. Lett.* **2007**, *90*, 132104.
[34] D. H. Kim, Y. Jang, Y. D. Park, K. Cho, *Langmuir* **2005**, *21*, 3203.
[35] F. Gholamrezaie, A.-M. Andringa, W. S. C. Roelofs, A. Neuhold, M. Kemerink, P. W. M. Blom, D. M. de Leeuw, *Small* **2012**, *8*, 241.
[36] M. Salinas, C. M. Jäger, A. Y. Amin, P. O. Dral, T. Meyer-Friedrichsen, A. Hirsch, T. Clark, M. Halik, *J. Am. Chem. Soc.* **2012**, *134*, 12648.

© 2021 The Authors. Advanced Materials Interfaces published by Wiley-VCH GmbH

[37] S. Kobayashi, T. Nishikawa, T. Takenobu, S. Mori, T. Shimoda, T. Mitani, H. Shimotani, N. Yoshimoto, S. Ogawa, Y. Iwasa, *Nat. Mater.* **2004**, *3*, 317.
[38] M. Aghamohammadi, R. Rödel, U. Zschieschang, C. Ocal, H. Boschker, R. T. Weitz, E. Barrena, H. Klauk, *ACS Appl. Mater. Interfaces* **2015**, *7*, 22775.
[39] Y. Wang, T. Hasegawa, H. Matsumoto, T. Mori, T. Michinobu, *Adv. Mater.* **2018**, *30*, 1707164.
[40] D. Boudinet, M. Benwadih, S. S. S. S. Altazin, J.-M. M. Verilhac, E. De Vito, C. Serbutoviez, G. Horowitz, A. Facchetti, *J. Am. Chem. Soc.* **2011**, *133*, 9968.
[41] H. Sugimura, K. Hayashi, N. Saito, N. Nakagiri, O. Takai, *Appl. Surf. Sci.* **2002**, *188*, 403.
[42] R. J. Kline, M. D. McGehee, M. F. Toney, R. J. Kline, M. D. McGehee, M. F. Toney, *Nat. Mater.* **2006**, *5*, 222.
[43] L. A. Majewski, R. Schroeder, M. Grell, P. A. Glarvey, M. L. Turner, *J. Appl. Phys.* **2004**, *96*, 5781.
[44] D. H. Kim, Y. D. Park, Y. Jang, H. Yang, Y. H. Kim, J. I. Han, D. G. Moon, S. Park, T. Chang, C. Chang, M. Joo, C. Y. Ryu, K. Cho, *Adv. Funct. Mater.* **2005**, *15*, 77.
[45] H.-L. Cheng, Y.-S. Mai, W.-Y. Chou, L.-R. Chang, X.-W. Liang, *Adv. Funct. Mater.* **2007**, *17*, 3639.
[46] T. N. Krauss, E. Barrena, D. G. de Oteyza, X. N. Zhang, J. Major, V. Dehm, F. Würthner, H. Dosch, *J. Phys. Chem. C* **2009**, *113*, 4502.
[47] E. Metwalli, D. Haines, O. Becker, S. Conzone, C. G. Pantano, *J. Colloid Interface Sci.* **2006**, *298*, 825.
[48] C. Gaul, S. Hutsch, M. Schwarze, K. S. Schellhammer, F. Bussolotti, S. Kera, G. Cuniberti, K. Leo, F. Ortmann, *Nat. Mater.* **2018**, *17*, 439.
[49] M. L. Tietze, J. Benduhn, P. Pahner, B. Nell, M. Schwarze, H. Kleemann, M. Krammer, K. Zojer, K. Vandewal, K. Leo, *Nat. Commun.* **2018**, *9*, 1182.
[50] M. Schwarze, C. Gaul, R. Scholz, F. Bussolotti, A. Hofacker, K. S. Schellhammer, B. Nell, B. D. Naab, Z. Bao, D. Spoltore, K. Vandewal, J. Widmer, S. Kera, N. Ueno, F. Ortmann, K. Leo, *Nat. Mater.* **2019**, *18*, 242.
[51] C. Celle, C. Suspene, J. Simonato, S. Lenfant, M. Ternisien, D. Vuillaume, *Org. Electron.* **2009**, *10*, 119.
[52] W. Melitz, J. Shen, A. C. Kummel, S. Lee, *Surf. Sci. Rep.* **2011**, *66*, 1.
[53] R. A. Kendall, E. Aprà, D. E. Bernholdt, E. J. Bylaska, M. Dupuis, G. I. Fann, R. J. Harrison, J. Ju, J. A. Nichols, J. Nieplocha, T. P. Straatsma, T. L. Windus, A. T. Wong, *Comput. Phys. Commun.* **2000**, *128*, 260.
[54] T. Yanai, D. P. Tew, N. C. Handy, *Chem. Phys. Lett.* **2004**, *393*, 51.
[55] Y. Tawada, T. Tsuneda, S. Yanagisawa, T. Yanai, K. Hirao, *J. Chem. Phys.* **2004**, *120*, 8425.
[56] T. H. Dunning, *J. Chem. Phys.* **1989**, *90*, 1007.
[57] R. A. Kendall, T. H. Dunning, R. J. Harrison, *J. Chem. Phys.* **1992**, *96*, 6796.
[58] E. R. Davidson, *Chem. Phys. Lett.* **1996**, *260*, 514.
[59] S. Grimme, J. Antony, S. Ehrlich, H. Krieg, *J. Chem. Phys.* **2010**, *132*, 154104.
[60] R. Ditchfield, W. J. Hehre, J. A. Pople, *J. Chem. Phys.* **1971**, *54*, 724.
[61] F. L. Hirshfeld, *Theor. Chim. Acta* **1977**, *44*, 129.
[62] J. P. Ritchie, *J. Am. Chem. Soc.* **1985**, *107*, 1829.
[63] J. P. Ritchie, S. M. Bachrach, *J. Comput. Chem.* **1987**, *8*, 499.
[64] M. J. Frisch, G. W. Trucks, H. B. Schlegel, G. E. Scuseria, M. A. Robb, J. R. Cheeseman, G. Scalmani, V. Barone, G. A. Petersson, H. Nakatsuji, X. Li, M. Caricato, A. V. Marenich, J. Bloino, B. G. Janesko, R. Gomperts, B. Mennucci, H. P. Hratchian, J. V. Ortiz, A. F. Izmaylov, J. L. Sonnenberg, D. Williams-Young, F. Ding, F. Lipparini, F. Egidi, J. Goings, B. Peng, A. Petrone, T. Henderson, D. Ranasinghe, et al., Gaussian 16, Revision C.01, Gaussian, Inc., Wallingford CT **2016**.
[65] R. Scholz, R. Luschtinetz, G. Seifert, T. Jägeler-Hoheisel, C. Körner, K. Leo, M. Rapacioli, *J. Phys. Condens. Matter* **2013**, *25*, 473201.

© 2021 The Authors. Advanced Materials Interfaces published by Wiley-VCH GmbH